PAPER

Far-infrared absorption spectra of synthetically-prepared, ligated metal clusters with Au₆, Au₈, Au₉ and Au₆Pd metal cores†

Jason F. Alvino,[a] Trystan Bennett,[a] David Anderson,[b] Baira Donoeva,[b] Daniil Ovoshchnikov,[b] Rohul H. Adnan,[bc] Dominique Appadoo,[d] Vladimir Golovko,*[b] Gunther Andersson*[e] and Gregory F. Metha*[a]

The far infra-red absorption spectra of a series of chemically synthesised, atomically precise phosphine-stabilised gold cluster compounds have been recorded using synchrotron light for the first time. Far-IR spectra of the $Au_6(Ph_2P(CH_2)_3PPh_2)_4(NO_3)_2$, $Au_8(PPh_3)_8(NO_3)_2$, $Au_9(PPh_3)_8(NO_3)_3$, and $Pd(PPh_3)Au_6(PPh_3)_6(NO_3)_2$ clusters reveal a complex series of peaks between 80 and 475 cm^{-1}, for which all significant peaks can be unambiguously assigned by comparison with Density Functional Theory (DFT) geometry optimisations and frequency calculation. Strong absorptions in all spectra near 420 cm^{-1} are assigned to the P–Ph₃ stretching vibrations. Distinct peaks within the spectrum of each specific cluster are assigned to the cluster core vibrations: 80.4 and 84.1 cm^{-1} (Au₆) 165.1 and 166.4 cm^{-1} (Au₈), 170.1 and 185.2 cm^{-1} (Au₉), and 158.9, 195.2, and 206.7 cm^{-1} (Au₆Pd). The positions of these peaks are similar to those observed to occur for the neutral Au₇ cluster in the gas phase (*Science*, 2008, **321**, 674–676). Au–P stretching vibrations only occur for Au₆ near 420 cm^{-1}, although they appear near 180 cm^{-1} for Au₆Pd and involve gold core vibrations.

Introduction

Over the past decade there has been great interest shown in the size-dependent chemical properties of metal clusters deposited onto active surfaces, particularly with a focus on catalysis. Most of this work has involved the study of size-selected clusters produced in the gas phase and subsequently deposited, or soft-landed, onto appropriately prepared surfaces. For example, Heiz and co-workers were able to utilise this approach to demonstrate that Au₈ clusters deposited onto an MgO surface were able to oxidise CO at temperatures as low as 140 K, and also show that smaller clusters were inactive.[1] Less common are studies that involve the preparation of ligand-stabilised metal clusters *via* chemical synthesis, immobilisation of these onto a support, and the subsequent activation of the cluster cores by removal of some, or all, of the ligands. Clearly, a key step with this approach

is the careful monitoring of the ligand removal process and to ensure that the clusters remain isolated on the surface (*i.e.* not agglomerated). Using synchrotron-based XPS, we have recently shown that atomically precise phosphine-stabilised gold clusters containing the gold cores of Au₈, Au₉ and Au₁₁ can be chemically synthesised, deposited onto titania surfaces and treated to remove some of the ligands.[2] The use of surface XPS has proven useful to follow changes in electronic structures of these systems. This work inspired us to explore other spectroscopic techniques for identifying the breaking and formation of chemical bonds that are expected to occur following cluster preparation, deposition and activation on a surface.

Infra-red spectroscopy is commonly used to observe the vibrational frequencies of key functional groups to monitor changes in chemical bonding during chemical synthesis. Despite recent, yet significant attention of the scientific community to chemical synthesis and characterisation of atomically precise gold-containing clusters (both thiol- and phosphine-protected), detailed IR studies of these systems are missing in the literature. This could be due to significant difficulties associated with acquisition of high-quality data across a wide range of frequencies necessary for detailed investigation. As pointed out by Stellwagen *et al.*, "the Au–S related peaks lie at even lower energies (220 cm^{-1}), and fall outside the range of our FT-IR spectrometer. In general the Au–S vibrations are very weak and difficult to observe".[3] Other relevant literature reports have

[a]*Department of Chemistry, University of Adelaide, South Australia 5005, Australia. E-mail: greg.metha@adelaide.edu.au; Fax: +61 8 8303 4358; Tel: +61 8 8303 5943*

[b]*The MacDiarmid Institute for Advanced Materials and Nanotechnology, Department of Chemistry, University of Canterbury, Christchurch 8140, New Zealand*

[c]*Chemistry Department, University of Malaya, 50603 Kuala Lumpur, Malaysia*

[d]*Australian Synchrotron, 800 Blackburn Road, Clayton, Vic 3168, Australia*

[e]*School of Chemical & Physical Sciences, Flinders University, G.P.O. Box 2100, Adelaide, South Australia 5001, Australia*

† Electronic supplementary information (ESI) available. See DOI: 10.1039/c3ra44803g

focused on FTIR investigations of Au–S vibrations for much larger (>1.5 nm), thiolate protected gold nanoparticles, where the metal cores were not defined with atomic precision.[4,5] Smaller clusters (up to 40 Au atoms) were shown to have intense optical activity due to metal-based transitions in the near-infrared region.[6] Earlier infra-red studies of chemically-synthesised, atomically precise ultra-small metal clusters indicate that strong metal–ligand bond vibrations appear at 450 cm^{-1} for phosphine-stabilised clusters.[7] At the same time, higher frequency modes associated with uncoordinated counter-ions were also observed. For example, in the case of Au$_8$Pt(PPh$_3$)$_8$(NO$_3$)$_2$ the band at 1360 cm^{-1} was assigned to NO$_3^-$.[7] Lower frequency bands (*i.e.* <400 cm^{-1}) have been observed in earlier studies of metal cluster carbonyl clusters (*e.g.* Ru$_3$(CO)$_{12}$) but these features were not generally attributed to specific modes except in a few highly symmetric cases.[8] These low frequency modes are generally expected to involve vibrational motions of the cluster core which will be very weak in intensity.

Recently, Fielicke and co-workers have applied IR-action spectroscopy using the FELIX tuneable IR-free electron laser to reveal low frequency vibrations of size-specific metal clusters produced in the gas phase by laser ablation. Multiple IR photons are used to resonantly dissociate rare gas atoms (usually Ar or Kr) attached to anionic, neutral and cationic clusters prepared under supersonically-cooled molecular beam conditions. Detection by time-of-flight mass spectrometry allows unambiguous spectral assignments to specifically-sized metal clusters. In combination with Density Functional Theory (DFT) calculations, these workers have been able to identify IR-active cluster vibrations. In cases where two or more isomers are feasible, it has been possible to correlate the observed spectral features to a specific isomer, or isomers. Pertinent examples include Au$_7$, Au$_{19}$ and Au$_{20}$,[9] and Y-doped Au clusters.[10–12]

Inspired by the possibility of identifying low frequency vibrational modes of ligand-stabilised clusters by comparison with DFT calculations, we have undertaken the measurement of low intensity, low frequency vibrational modes of chemically-synthesised, atomically-precise ligand-stabilised metal clusters using a high intensity synchrotron-based far-IR source. Herein we report a methodology for obtaining reproducible spectra of ligand-protected clusters, which has been developed over several visits to the Far-IR beamline at the Australian Synchrotron. We have focused on the gold cluster cores of Au$_6$, Au$_8$, Au$_9$ and Au$_6$Pd stabilised by phenylphosphine-based ligands. The experimentally obtained spectra are compared with DFT-computed vibrational frequency calculations of the full cluster, including all ligands. This allows us to identify key features in the IR spectrum that can be assigned to specific vibrational motions of the metal core, as well as vibrations between the metal atoms and ligands (*i.e.* Au–P bonds). We note the very recent report of a DFT investigation of thiol protected, size specific gold clusters showing calculated IR and Raman spectra for the clusters Au$_4$.[13]

Experimental & computational procedures

The Au$_6$(Ph$_2$P(CH$_2$)$_3$PPh$_2$)$_4$(NO$_3$)$_2$ cluster (CSD Refcode BOTSOS; hereafter referred to as Au$_6$) was prepared according to the

procedure reported by Van der Velden *et al.*[14] The Au$_8$(PPh$_3$)$_8$(NO$_3$)$_2$ cluster (CSD Refcode OPAUPF; hereafter referred to Au$_8$) was synthesised following protocol described by Van der Velden *et al.*[15] The Au$_9$(PPh$_3$)$_8$(NO$_3$)$_3$ cluster (CSD Refcode MIVPOX; hereafter referred to as Au$_9$) was prepared following the method described by Wen *et al.*[16] The Pd(PPh$_3$)Au$_6$(PPh$_3$)$_6$(NO$_3$)$_2$ cluster (CSD Refcode UHIPEG; hereafter referred to as Au$_6$Pd) was prepared following the procedure of Takata *et al.*,[17] which gives higher yield of this cluster than earlier reported (along with its crystal structure) by Quintilio *et al.*[18] Note that for the Au$_6$Pd cluster, the crystal structure utilised referred to the similar Pd(PPh$_3$)Au$_6$(PPh$_3$)$_6$(PF$_6$)$_2$, which employs a PF$_6^-$ counter-ion, however this is not expected to have affected the cluster geometry given the omission of counter-ions in the calculation.

Samples were prepared by pressing 50 mg of pure powdered cluster material into a pellet. Their far-IR absorption spectra were recorded using the IFS125 Bruker FT spectrometer located at the Far-IR beamline, at the Australian Synchrotron. The transmission spectrum for each sample was recorded from 50 to 650 cm^{-1}, at 1 cm^{-1} resolution utilising the synchrotron light source (200 mA in top-up mode), a 6 micron thick multilayer Mylar beamsplitter in combination with a Si bolometer detector; the bolometer was equipped with a 800 cm^{-1} far-IR cut-on cold-filter consisting of a 13 micron PE film overlaid with 6 micron diamond scatter layer. Samples were recorded at room temperature and again at 77 K with no discernible differences between spectra; all spectra were baseline corrected.

Geometry optimisation and harmonic vibrational frequency calculations of the gold cluster compounds, including all ligands, were undertaken using the M06 density functional[19] in the Gaussian 09 suite of programs.[20] Starting geometries were taken from crystal structures obtained from X-ray diffraction patterns of the synthesised clusters (reported earlier by others or ourselves) which were deposited in the Cambridge Crystallographic Database.[21] All counter ions were removed, with the appropriate number of electrons removed from the calculations to balance the charge. All atoms were treated using the LanL2DZ basis set and related Effective Core Potentials (ECP).[22–25] All optimisations were
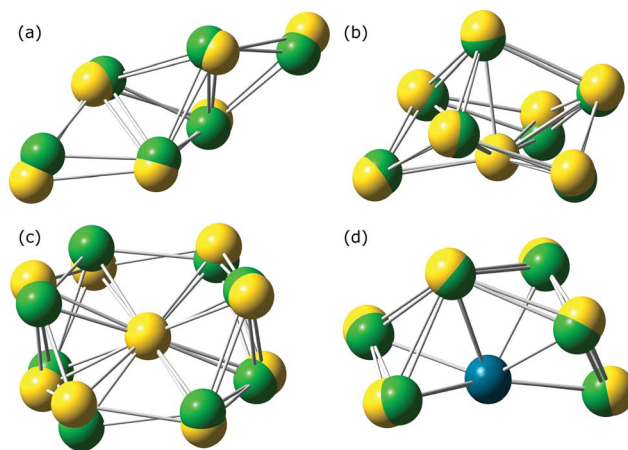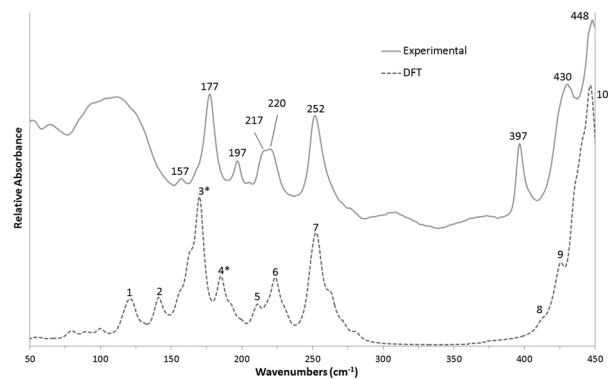

Fig. 1 X-ray crystal structures (green) and DFT optimised structures (yellow) for the (a) Au$_6$, (b) Au$_8$, (c) Au$_9$, and (d) Au$_6$Pd clusters. Ligand groups are omitted for clarity.
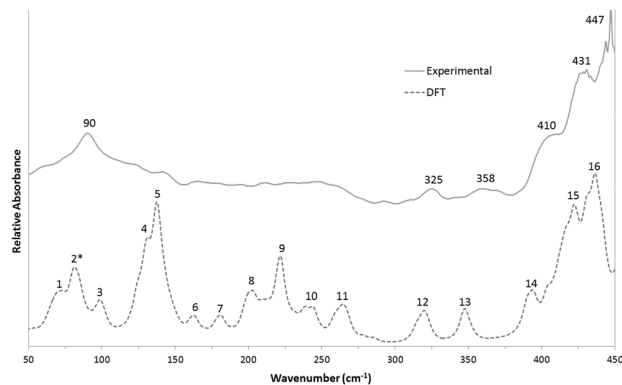
Fig. 2 Experimental (solid line) and simulated (dotted line) far-IR spectrum of the Au_6 cluster.

Fig. 4 Experimental (solid line) and simulated (dotted line) far-IR spectrum of the Au_9 cluster.
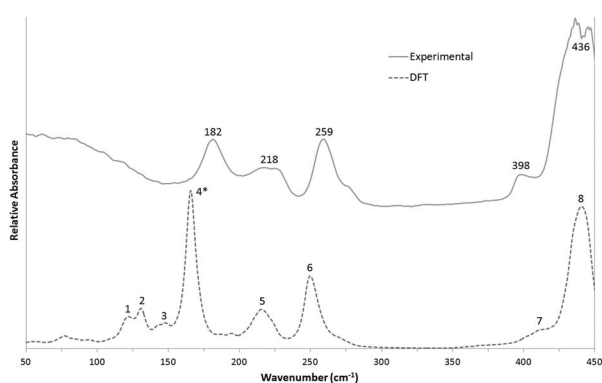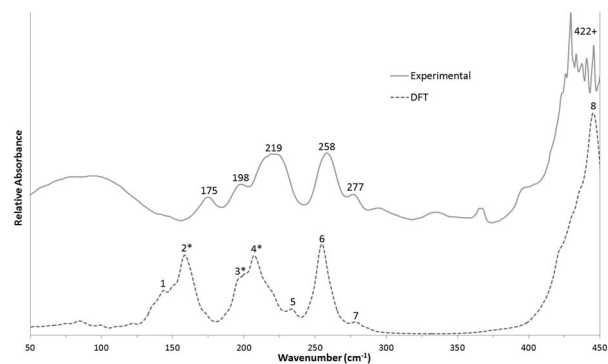

Fig. 3 Experimental (solid line) and simulated (dotted line) far-IR spectrum of the Au_8 cluster.

Fig. 5 Experimental (solid line) and simulated (dotted line) far-IR spectrum of the Au_6Pd cluster.

performed with no symmetry constraints, *i.e.* in the C_1 point group. Each optimised geometry was followed by a harmonic frequency calculation to confirm that the geometry was a true minimum with no imaginary frequencies. The exception to this was the Au_8 structure, which was optimised to a stationary point with three low-frequency imaginary frequencies (42.6, 30.8, and 26.1 cm^{-1}). Inspection of the imaginary modes reveal that they correspond to slight rotations of phenyl groups and despite numerous attempts at re-optimisation using finer grid sizes and alternative minimisation algorithms we were unable to eliminate them. In light of the small magnitude and local nature of these vibrations, we conclude that they do not adversely impact on our assessment of the core cluster vibrations which are of primary interest here. To obtain the predicted IR spectra, each stick spectrum is convoluted with a Gaussian line shape function with 8 cm^{-1} full width at half maximum using the GaussView 5 program. Full geometric information for each optimised structure is provided in the accompanying ESI file.†

Results & discussion

The optimised structures for the cluster compounds of Au_6, Au_8, Au_9, and Au_6Pd are shown in Fig. 1, with only Au and Pd atoms shown for clarity. Superimposed on these structures are the corresponding crystal structures. The superimposed structures

presented in Fig. 1 illustrate the very close match between "gas-phase" and condensed phase geometries. There is a trend across all molecules towards longer bond lengths, as the molecule is optimised from the crystal structure starting position, to its final gas-phase geometric minima.

The predicted spectra over the range 50–450 cm^{-1} for the Au_6, Au_8, Au_9 and Au_6Pd clusters are shown in Fig. 2–5 as dotted lines. Note that these spectra only include the calculated fundamental vibrations and so do not include overtones or combination bands. The number of calculated transitions is vast, with more than 150 transitions occurring in the region presented above. Given the large number of vibrations to consider, Tables 1–4 list the calculated frequency modes up to 450 cm^{-1} that pass one of two selection criteria. Firstly, in order to distinguish the normal modes involving the cluster core vibrations from other low frequency modes, we have identified the normal coordinate motions that involve significant motion of the Au, Pd, and P atoms. These appear in Tables 1–4 as a percentage of the total non-mass-weighted atomic motion (*i.e.* %Au and %P). Secondly, the tables include any normal mode that has significant calculated IR intensity of >1 km mol^{-1}. These modes are listed either individually or as groups of peaks and numbered sequentially starting at low energy. This peak numbering scheme in Tables 1–4 is the same as the one used in the simulated spectra presented in Fig. 2–5. For the calculated

Table 1 Summary of all calculated contributing transitions for the Au_6 cluster and their assignment to the predicted spectral peaks, as well as their assignment to the observed far-IR spectrum of the cluster, and a brief description of the assigned transition modes

#	Peak (cm^{-1})	Contributing vibrations (cm^{-1})	IR intensity ($km\ mol^{-1}$)	%Au motion	%P motion	Assigned (cm^{-1})	Mode description
1	73	69.6	1.3	6.1%	4.8%		
		72.9	1.4	8.7%	4.6%		
2	81	80.4*	4.7	17.1%	5.1%	90.2	Au core distortion
		81.1	1.1	8.6%	6.3%		
		84.1*	4.3	16.4%	6.6%		
		87.9	0.8	16.8%	5.0%		
3	99	98.8	3.7	5.6%	5.4%		
		104.9	0.1	14.5%	5.7%		
4	131	129.9	3.6	3.4%	7.3%		
		130.5	6.1	4.9%	6.6%		
5	138	137.2	5.3	4.8%	5.9%		
		137.9	9.6	6.7%	7.0%		
		139.0	1.8	4.3%	7.4%		
		142.8	2.9	6.1%	6.9%		
6	163	162.6	1.3	1.9%	4.0%		
		163.9	1.1	13.3%	4.6%		
7	180	179.8	1.1	2.2%	3.3%		
		181.8	2.0	1.3%	3.0%		
8	203	198.3	1.9	0.0%	2.8%		
		200.1	2.3	0.8%	1.8%		
		203.5	3.7	0.7%	2.1%		
9	222	219.3	1.5	0.0%	1.4%		
		220.9	1.3	0.0%	1.2%		
		222.0	7.8	0.0%	1.4%		
10	244	238.5	2.9	0.0%	1.4%		
		244.2	3.6	0.0%	1.6%		
11	265	263.3	1.0	0.0%	1.5%		
		264.2	1.1	0.0%	2.0%		
		265.3	1.1	0.0%	1.9%		
12	320	314.8	1.7	0.0%	7.3%	325.4	P_2Ph_4–$(CH_3)_3$ wag – ligand 1
		318.9	1.5	0.0%	8.0%		P_2Ph_4–$(CH_3)_3$ wag – ligand 2
		319.9	1.4	0.7%	9.4%		P_2Ph_4–$(CH_3)_3$ wag – ligand 3
		321.7	1.9	0.0%	8.2%		P_2Ph_4–$(CH_3)_3$ wag – ligand 4
13	348	347.2	3.4	0.0%	10.7%	357.7	P–$(CH_2)_3$–P distortion
		347.8	1.3	0.0%	11.4%		
14	394	390.0	3.6	0.9%	15.1%	410.3	P–C–C–C–P bend
		394.3	4.2	0.8%	15.1%		
15	422	421.7	4.9	0.5%	13.2%	430.5	Au–P stretch
		422.3	4.6	0.0%	11.1%		P–Ph stretch
16	436	429.8	5.2	1.2%	16.3%	446.9	Au–P stretch
		431.3	6.3	1.2%	16.5%		Au–P stretch
		436.4	14.6	0.0%	16.6%		P–Ph stretch
		441.0	7.7	0.8%	17.0%		P–Ph stretch

transitions that are assigned to experimental features, a brief description of the normal mode also appears in Tables 1–4. For each cluster, several key, core vibrations involving the metal atoms are pictorially represented in Fig. 6–9, and the peaks corresponding to these transitions are highlighted within Fig. 2–5 as well as Tables 1–4 with an asterisk.

Table 2 Summary of all calculated contributing transitions for the Au$_8$ cluster and their assignment to the predicted spectral peaks, as well as their assignment to the observed far-IR spectrum of the cluster, and a brief description of the assigned transition modes

#	Peak (cm^{-1})	Contributing vibrations (cm^{-1})	IR intensity (km mol^{-1})	%Au motion	%P motion	Assigned (cm^{-1})	Mode description
1	122	119.1	3.4	5.2%	4.6%		
		121.1	1.7	3.8%	3.9%		
		122.2	2.0	3.2%	3.5%		
		124.4	1.9	4.8%	4.3%		
2	131	131.1	9.3	7.5%	5.6%		
3	148	142.6	2.9	10.7%	5.2%		
		147.4	1.7	12.7%	5.0%		
		148.7	1.9	12.6%	4.8%		
4	166	165.1*	23.9	20.3%	2.7%	181.8	Au core distortion
		166.4*	23.9	20.2%	2.9%		
		171.6	3.2	16.7%	1.6%		
5	216	210.3	1.5	0.0%	0.8%	217.9	Ph rock
		210.9	1.7	0.0%	1.4%		
		214.5	2.8	0.0%	1.2%		
		215.8	1.2	0.0%	1.3%		
		217.0	1.6	0.5%	1.5%		
		219.1	1.8	0.0%	1.3%		
6	250	247.4	4.1	0.0%	1.1%	258.9	Ph rock
		248.3	3.8	0.0%	0.9%		
		249.4	4.1	0.0%	1.2%		
		249.9	3.3	0.0%	1.3%		
		250.2	1.7	0.0%	1.4%		
		251.7	3.1	0.0%	1.0%		
		253.1	3.9	0.0%	1.3%		
7	411 (shoulder)	410.5	0.5	0.0%	1.9%	398.2	Ph twist
		411.5	0.4	0.0%	0.7%		
8	441	428.9–445.8	Avg. 3.9	Avg. 0%	Avg. 13%	436.3	PPh$_3$ distortion

Also shown in Fig. 2–5 are the experimental IR spectra for Au$_6$, Au$_8$, Au$_9$ and Au$_6$Pd (solid line). All clusters exhibit an intense absorption near 440 cm^{-1} and a broad featureless absorption below 130 cm^{-1}, except Au$_6$ which has a feature ~90 cm^{-1}. We are confident that the spectrometer is operating correctly in this region since we were able to observe characteristic features present in this region for the mono-gold compound (AuPPh$_3$Cl) which were in agreement with earlier reported data.[26] The spectrum of AuPPh$_3$Cl (see Fig. S1 in ESI†) was recorded under similar conditions to other spectra in this study, confirming that the instrumentation set-up is capable of data acquisition in this region. The spectrum shows very little difference when recorded under reduced temperature conditions (77 K) thus removing the possibility of phonon bands being confused for features due to molecular vibrations. Nevertheless, it seems likely that the broad features arise from dampening of the low frequency vibrations due to the condensed phase nature of the sample as the calculated spectrum is generated under gas phase (*i.e.* isolated molecule) conditions.

The Au$_8$, Au$_9$ and Au$_6$Pd spectra also display several distinct peaks between 180 and 260 cm^{-1}. The higher energy feature at

430 cm^{-1} has been previously observed in the pure ligand, PPh$_3$, and identified as being due to P–Ph$_3$ vibrations.[27] This is consistent with our calculations, although we also show that Au–P stretches occur in the same spectral region (*vide infra*). Some of the intense features near 450 cm^{-1} for Au$_6$, Au$_8$ and Au$_6$Pd reach 100% absorption but no attempt was made to reduce the concentration due to the low significance of this spectral region.

To the best of our knowledge, the detailed far-IR spectra below 300 cm^{-1} reported here are the first ever high quality dataset for chemically synthesised, atomically precise gold clusters, enabling detailed analysis of their features. Discussed below are the assignments made for each of the observed peaks, which are based upon calculated vibrational frequencies and predicted intensities (Tables 1–4).

A. The Au$_6$ cluster

The experimental Au$_6$ spectrum (Fig. 2) clearly consists of two main peaks (including a shoulder) above 400 cm^{-1}, as well as a broad peak centred at 90 cm^{-1}. The former peaks closely match the calculated spectrum, which predicts three transitions at

Table 3 Summary of all calculated contributing transitions for the Au_9 cluster and their assignment to the predicted spectral peaks, as well as their assignment to the observed far-IR spectrum of the cluster, and a brief description of the assigned transition modes

#	Peak (cm^{-1})	Contributing vibrations (cm^{-1})	IR intensity (km mol^{-1})	%Au motion	%P motion	Assigned (cm^{-1})	Mode description
1	121	116.0	2.1	1.9%	1.7%		
		119.3	2.7	6.0%	2.4%		
		120.0	2.0	5.6%	2.3%		
		122.9	4.6	3.6%	1.7%		
2	141	140.9	7.2	8.3%	5.8%	157.2	Au core distortion
3	170	162.8	11.2	8.1%	4.6%	177.4	Au core distortion
		170.1*	28.0	17.7%	3.3%		
4	185	185.2*	11.2	17.7%	1.7%	196.7	Au core distortion
5	211	210.7	2.0	0.0%	1.1%	216.5	Ph rock
		211.0	3.2	0.0%	0.8%		
6	224	217.6	2.7	0.0%	1.2%	219.8	Ph rock
		222.2	2.3	0.0%	0.7%		
		223.7	5.6	0.0%	0.7%		
		224.2	3.1	0.0%	1.4%		
7	253	248.9	6.6	0.0%	1.0%	251.7	PPh$_3$ distortion
		251.6	6.2	0.0%	0.8%		
		252.2	3.2	0.0%	0.6%		
		253.9	9.9	0.0%	0.9%		
8	411 (shoulder)	411.8	0.9	0.0%	1.0%	396.8	Ph twist
		412.2	0.7	0.0%	1.0%		
9	426	424.5	1.5	0.0%	3.2%	430.0	Ph twist
		424.6	1.9	0.0%	3.0%		
		425.4	3.6	0.0%	4.7%		
		425.5	1.9	0.0%	2.5%		
10	447	435.2–448.8	Avg. 8.1	Avg. 0%	Avg. 13%	447.9	PPh$_3$ distortion

393.7 cm^{-1} (#14) due to P–(CH$_2$)$_3$–P bending, at 422.3 cm^{-1} and 436.3 cm^{-1} (#15 & #16 respectively) both due to a combination of the Au–P and P–Ph$_3$ stretches.

The observed peak at 90 cm^{-1} corresponds to a group of calculated transitions around 84 cm^{-1} (#2), which are all due to metal core vibrations. All four transitions have significant Au motions of 9–17% (see Table 1) and the displacement vectors for the two most IR intense vibrations are shown in Fig. 6. This low frequency peak at 90 cm^{-1} is interesting since none of the other clusters have observable, nor calculated, core metal vibrational modes this low in frequency. The simulated spectrum also shows a strong peak with a shoulder at 138 cm^{-1} and 131 cm^{-1}, respectively (#5 & #4), both of which consist of several modes with moderate %Au motions (~5%) and significant IR intensities (A = 4–10). These peaks match the two shoulders (unlabelled) in the experimental spectrum near 120 and 148 cm^{-1}.

The experimental spectrum also shows two weaker peaks at 325 cm^{-1} and 358 cm^{-1}. These also appear in the calculated spectrum at 320 cm^{-1} (#12) and 348 cm^{-1} (#13) respectively, and correspond to distortions of the chelating P–(CH$_2$)$_3$–P ligands. The simulated spectra also show a number of peaks

(#6–11) in the region from 160 cm^{-1} to 265 cm^{-1}, which do not distinctly appear in the experimental spectrum. Only one of these transitions contains significant Au motion (#6 with 13% Au), with a low IR intensity (~1.1 km mol^{-1}), and the remainder are large-amplitude ligand vibrations. There are other transitions (<150 cm^{-1}) involving large amplitude motions spanning several ligand groups, that are calculated to have non-negligible IR intensities but do not appear in the spectrum. We suggest that given the condensed nature of the samples (*i.e.* pressed pellet) that these modes are more readily quenched than the core metal vibrations. Although we have no direct evidence for this, it is a common theme observed for all the other clusters (*vide infra*).

B. The Au$_8$ and Au$_9$ clusters

Both the Au$_8$ and Au$_9$ spectra display an intense peak at 440 cm^{-1}. These features are clearly reproduced in the associated simulated spectra. As mentioned above, the normal mode analysis indicates that these transitions ((#8) in the case of Au$_8$ and (#10) for Au$_9$) correspond to the P–Ph$_3$ stretching vibrations

Table 4 Summary of all calculated contributing transitions for the Au$_6$Pd cluster and their assignment to the predicted spectral peaks, as well as their assignment to the observed far-IR spectrum of the cluster, and a brief description of the assigned transition modes

#	Peak (cm^{-1})	Contributing vibrations (cm^{-1})	IR intensity (km mol^{-1})	%Au motion	%Pd motion	%P motion	Assigned (cm^{-1})	Mode description
1	144	135.7	2.6	2.8%	2.6%	4.1%		
		139.7	1.6	2.7%	1.5%	2.1%		
		142.3	1.4	3.3%	0.7%	2.1%		
		143.9	3.9	3.8%	2.4%	2.4%		
2	159	149.7	3.4	5.3%	2.7%	3.9%	174.5	Pd–Au–P stretch
		150.9	1.5	5.6%	0.7%	3.2%		P–Au–Au–P stretch
		156.0	2.2	5.8%	0.8%	2.6%		Metal core distortion
		157.1	4.1	6.8%	0.7%	4.0%		Pd–Au–P stretch
		158.9*	6.5	7.7%	1.1%	3.8%		Metal core distortion
		162.2	5.2	8.3%	1.9%	3.7%		P–Au–Au–P stretch
3	195 (shoulder)	195.2*	6.0	4.7%	2.5%	1.8%	197.7	Metal core distortion
		198.9	1.5	1.3%	1.4%	2.2%		PPh$_3$ rotation
		200.8	1.8	4.8%	2.0%	1.9%		Pd–P stretch
4	207	201.1	2.6	1.9%	1.6%	1.8%	218.9	PPh$_3$ rotation
		206.7*	9.0	8.0%	4.9%	1.0%		Metal core distortion
		210.1	3.7	0.5%	1.0%	1.5%		Ph rock
		211.2	1.7	2.6%	1.4%	1.1%		PPh$_3$ rotation
		214.5	1.5	8.4%	8.5%	1.8%		Pd–P stretch
5	234	233.8	2.1	0.0%	0.0%	0.9%		Ph rock
6	255	252.1	3.1	0.0%	0.0%	1.0%	257.9	Ph rock
		253.5	3.2	0.0%	0.0%	1.1%		
		254.3	4.2	0.0%	0.0%	1.1%		
		254.9	1.4	0.4%	0.3%	1.7%		
		255.7	3.3	0.0%	0.4%	1.9%		
		256.8	3.8	0.0%	0.0%	1.3%		
		260.6	2.5	0.0%	0.0%	0.6%		
7	278	277.6	0.7	0.0%	0.0%	1.0%	276.7	Ph rotation
		279.6	0.4	0.0%	0.0%	1.3%		
8	445	421.1–449.2	Avg. 4.6	Avg. 0%	Avg. 0%	Avg. 11%	400–450+	PPh$_3$ distortion

with their high intensity arising from the large number of similar bonds – there are eight PPh$_3$ ligands per cluster core each giving rise to three P–Ph vibrations. The shoulder at 430 cm^{-1} in Au$_9$ matches a set of four similar transitions involving Ph-twisting vibrations (#9).

Both spectra exhibit distinct peaks at 398 cm^{-1}, which is much stronger in Au$_9$ compared to Au$_8$. Our calculations predict weak peaks for Au$_8$ (#7) and Au$_9$ (#8) that seem to match the position of this experimentally observed feature but not its intensity. These are due to a combination of two normal modes in each cluster, both involving phenyl group twisting vibrations. A similar mode for Au$_9$ is calculated at 426 cm^{-1} (#9), which corresponds to an intense feature at 430 cm^{-1} in the experimental spectrum.

The observed Au$_8$ spectrum has strong bands at 259 cm^{-1} and 182 cm^{-1}, and a weaker, broader transition centred at 218 cm^{-1}. Each of these peaks is simulated with excellent fit in both relative intensity and energy. The calculated peak at 250 cm^{-1} (#6), as well as the weaker peak at 216 cm^{-1} (#5), are due to the rocking motions of the phenyl (Ph) group. However,

the key feature in this region is the intense peak calculated at 166 cm^{-1} (#4), which is attributed to the two high intensity vibrations of the gold core. Vector displacements for these intense cluster core vibrations are shown in Fig. 7. We assign these calculated vibrations to the experimentally observed peak at 182 cm^{-1}.

The experimental spectrum of the Au$_9$ has an intense peak at 251 cm^{-1}, which matches a collection of PPh$_3$ distortion modes predicted by our calculations to be around 253 cm^{-1} (#7). Similarly, features observed at 217 cm^{-1} and 220 cm^{-1} are assigned to peaks at 211 (#5) and 224 cm^{-1} (#6), respectively, both being due to PPh$_3$ rocking vibrations.

Also for Au$_9$, the peak observed at 177 cm^{-1} matches the predicted peak at 170 cm^{-1} (#3), and the observed feature at 197 cm^{-1} matches the peak at 185 cm^{-1} (#4). Both of these peaks are of particular interest too, as their origin is due to the metal core vibrations. Fig. 8 illustrates displacement vectors corresponding to these core vibrations. Our calculations predict that these features should have high intensity which is in perfect agreement with experimental data. Finally, we assign

the small feature at 157 cm^{-1} to the single transition peak predicted to occur at 141 cm^{-1} (#2). Interestingly, this particular mode arises due to the vibration of the central Au atom (8% Au motion) relative to the ring of the other eight gold atoms around it and is calculated to have less intensity than the other gold core vibrations.

From the normal calculated mode analysis, there are two predicted transitions for the Au$_8$ cluster at 165 cm^{-1} and 166 cm^{-1} that involve the largest combined motion of the metal cluster core atoms (∼20% Au motion). Similarly, in the case of Au$_9$ cluster there are two predicted transitions at 170 cm^{-1} and 185 cm^{-1} that have significant gold core motion (∼18% Au motion). Importantly, the vibrational energy corresponding to the transitions responsible for these peaks is similar to that observed in the case of the gas-phase IR studies of Au$_7$–Kr cluster reported by Fielicke and co-workers.[9] Using IR-depletion spectroscopy, the authors observed three peaks at 165, 186 and 201 cm^{-1}, which correlated very well with their DFT-predicted spectrum (note that removal of the rare gas atom has very little effect on the vibrational frequencies of the remaining Au$_7$ cluster core). It was proposed that the cluster core (both with the Kr atom and without) has C_s-planar structure made up of 5 equilateral triangles and the three prominent vibrational peaks were assigned to various delocalised motions of all Au atoms in the cluster. It is interesting that the frequencies of the bare Au$_7$ cluster observed in gas phase are similar to the ones observed by

us for the cores of similarly sized, chemically-synthesised gold clusters that are protected by ligands and form extended crystalline lattices. This suggests that the bonding strengths within the metal cores for these two types of cluster systems are similar, despite having quite different geometric structures (*i.e.* 3D *vs.* 2D for clusters in the gas phase).

Below 140–150 cm^{-1} for both Au$_8$ and Au$_9$, the calculated spectra show a series of weaker peaks that do not resemble the experimental data. None of these are due to core cluster vibrations but involve a collection of vibrations comprising large-amplitude movement of the P–Ph$_3$ ligand groups that again, appear to be suppressed, consistent with that observed for Au$_6$.

C.   The Au$_6$Pd cluster

This spectrum is dominated by a broad peak extending from 400 to beyond 450 cm^{-1}, which is assigned to a plethora of intense PPh$_3$ distortions calculated to begin at 421 cm^{-1}. The Au$_6$Pd cluster is observed to have a series of strong and moderate bands at 277 (m), 258 (s), 219 (s), 198 (m) and 175 cm^{-1} (m). The predicted spectrum shows a range of peaks that appear to match the experimental spectrum except they are at slightly lower energy. Calculated peaks at 278 cm^{-1} (#7), 255 cm^{-1} (#6) and 234 cm^{-1} (#5) are due to the phenyl group
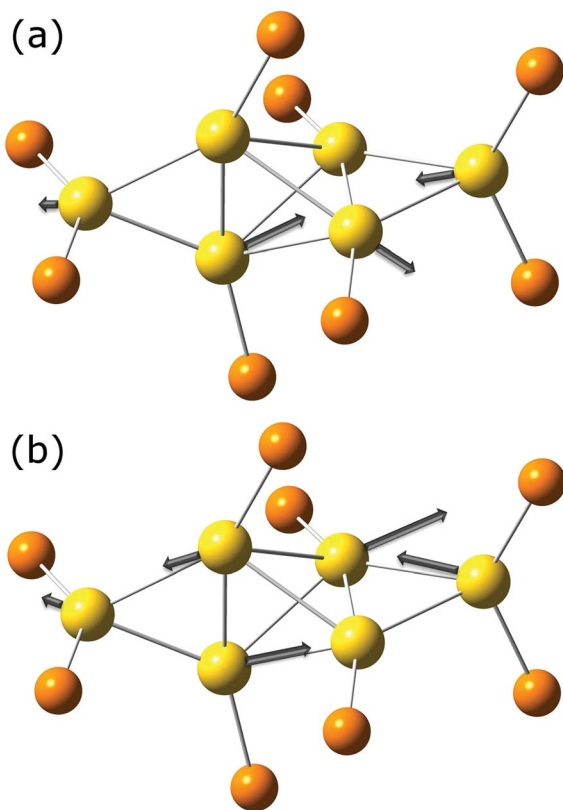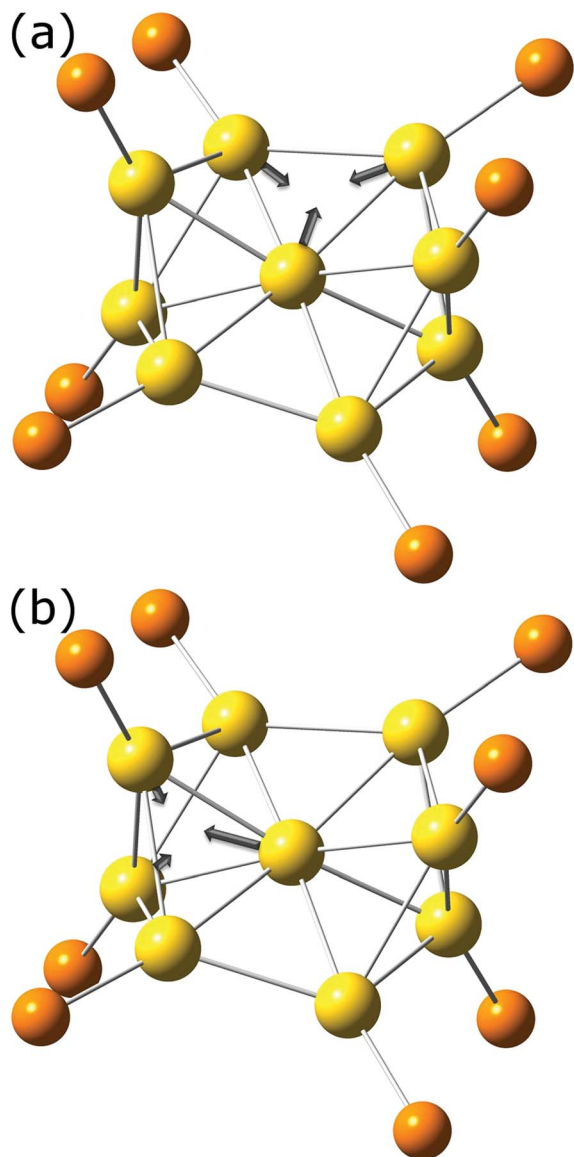

Fig. 6   Calculated normal mode displacements associated with the cluster core vibrations for Au$_6$ at (a) 80.4 cm^{-1} and (b) 84.1 cm^{-1}. Phenyl groups are omitted for clarity.
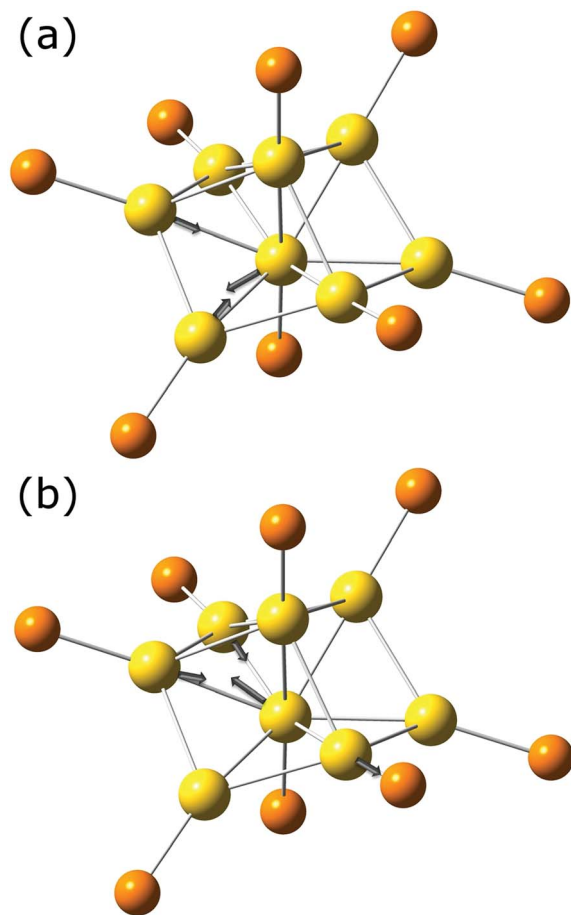
Fig. 7   Calculated normal mode displacements associated with the cluster core vibrations for Au$_8$ at (a) 165.1 cm^{-1} and (b) 166.4 cm^{-1}. Phenyl groups are omitted for clarity.

charge and geometry, and the presence of PPh_3 ligands, it is surprising that the vibrational frequencies are so similar between the naked metal cluster in the gas phase and our fully ligated cluster in solid state.
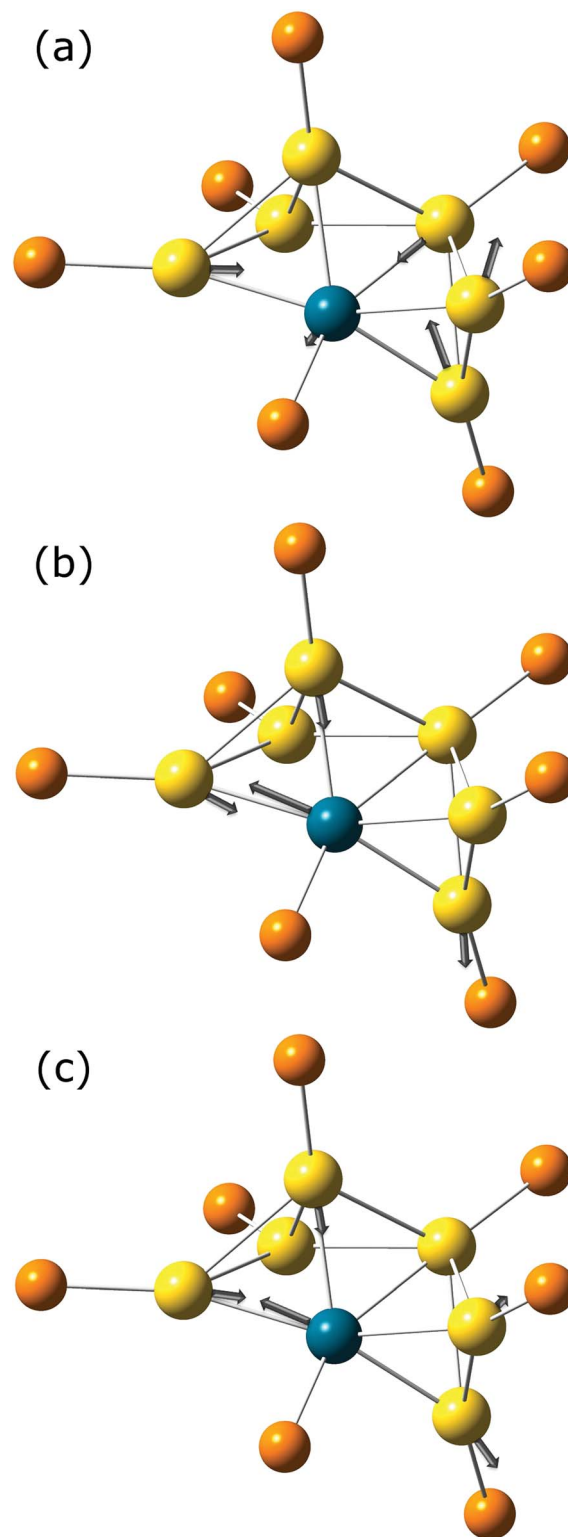

Fig. 8 Calculated normal mode displacements associated with the cluster core vibrations for Au_9 at (a) 170.1 cm^{-1} and (b) 185.2 cm^{-1}. Phenyl groups are omitted for clarity.

rotation and rocking ($\times 2$), respectively. We are assigning peaks #2, #3 and #4 to the lower energy three peaks seen in the experimentally obtained spectrum. Importantly, these vibrational modes involve a combination of Au and Pd motions. Specific transitions to note are at 159, 195 and 207 cm^{-1}, which have a total metal motion of >7%, with the Pd contribution ranging from 1 to 5%. The vector displacements for these modes are shown in Fig. 9. Finally, there is a weak peak experimentally observed at 360 cm^{-1}, which does not correlate to anything in our predicted spectrum.

We are aware of previously published FELIX IR data for a related metal cluster, namely neutral[10,11] and cationic[12] Au_6Y. The neutral structure is slightly distorted from planarity and this yields an IR spectrum with broad peaks from 75–220 cm^{-1}. The cationic structure has C_{3v} symmetry and has distinct peaks at 121 and 181 cm^{-1}. Again, given the difference in cluster core

Fig. 9 Calculated normal mode displacements associated with the cluster core vibrations for Au_6Pd at (a) 158.9 cm^{-1}, (b) 195.2 cm^{-1}, and (c) 206.7 cm^{-1}. Phenyl groups are omitted for clarity.

Consistent with that observed for all three pure gold clusters reported above, the spectrum of Au$_6$Pd is observed to contain a broad, featureless peak below 150 cm^{-1}, showing no resemblance to the calculated spectra. The large, multi-ligand transitions predicted to occur within this region appear to be suppressed, as postulated for the pure gold clusters above.

Conclusions

We have demonstrated that synchrotron-based, far-IR spectroscopy can be used to identify vibrational motions of chemically-synthesised, ligand-protected pure gold and mixed-metal cluster compounds. We have identified a transition near 180 cm^{-1} that involves gold cluster core vibrations for both Au$_8$ and Au$_9$. In the case of Au$_6$Pd, this transition is shifted to higher energy (218 cm^{-1}) implying that the presence of a Pd atom significantly affects gold cluster core $i.e.$ a strong heteroatom effect is evident. The related metal core transitions in the case of Au$_6$ cluster are observed at a significantly different position (90 cm^{-1}) to all other clusters in this study, which do not have IR-active metal core vibrations in this region. The experimental observations have been verified by comparison with predicted IR spectra based upon DFT-optimised structures.

Acknowledgements

References

1 B. Yoon, H. Häkkinen, U. Landman, A. S. Wörz, J.-M. Antonietti, S. Abbet, K. Judai and U. Heiz, *Science*, 2005, **307**, 403–407.

2 D. P. Anderson, J. F. Alvino, A. Gentleman, H. Al Qahtani, L. Thomsen, M. I. Polson, G. F. Metha, V. B. Golovko and G. G. Andersson, *Phys. Chem. Chem. Phys.*, 2013, **15**, 3917–3929.

3 D. Stellwagen, A. Weber, G. L. Bovenkamp, R. Jin, J. Bitter and C. S. Kumar, *RSC Adv.*, 2012, **2**, 2276–2283.

4 M. J. Hostetler, J. J. Stokes and R. W. Murray, *Langmuir*, 1996, **12**, 3604–3612.

5 M. J. Hostetler, J. E. Wingate, C.-J. Zhong, J. E. Harris, R. W. Vachet, M. R. Clark, J. D. Londono, S. J. Green, J. J. Stokes, G. D. Wignall, G. L. Glish, M. D. Porter, N. D. Evans and R. W. Murray, *Langmuir*, 1998, **14**, 17–30.

6 T. G. Schaaff and R. L. Whetten, *J. Phys. Chem. B*, 2000, **104**, 2630–2641.

7 J. J. Bour, R. P. F. Kanters, P. P. J. Schlebos and J. J. Steggerda, *Recl. Trav. Chim. Pays-Bas*, 1988, **107**, 211–215.

8 D. M. Adams and I. D. Taylor, *J. Chem. Soc., Faraday Trans. 2*, 1982, **78**, 1561–1571.

9 P. Gruene, D. M. Rayner, B. Redlich, A. F. G. van der Meer, J. T. Lyon, G. Meijer and A. Fielicke, *Science*, 2008, **321**, 674–676.

10 L. Lin, P. Claes, P. Gruene, G. Meijer, A. Fielicke, M. T. Nguyen and P. Lievens, *ChemPhysChem*, 2010, **11**, 1932–1943.

11 L. Lin, T. Höltzl, P. Gruene, P. Claes, G. Meijer, A. Fielicke, P. Lievens and M. T. Nguyen, *ChemPhysChem*, 2008, **9**, 2471–2474.

12 L. Lin, P. Claes, T. Holtzl, E. Janssens, T. Wende, R. Bergmann, G. Santambrogio, G. Meijer, K. R. Asmis, M. T. Nguyen and P. Lievens, *Phys. Chem. Chem. Phys.*, 2010, **12**, 13907–13913.

13 A. Tlahuice-Flores, R. L. Whetten and M. Jose-Yacaman, *J. Phys. Chem. C*, 2013, **117**, 12191–12198.

14 J. W. A. Van der Velden, J. J. Bour, J. J. Steggerda, P. T. Beurskens, M. Roseboom and J. H. Noordik, *Inorg. Chem.*, 1982, **21**, 4321–4324.

15 J. W. A. Van der Velden, J. J. Bour, W. P. Bosman and J. H. Noordik, *Inorg. Chem.*, 1983, **22**, 1913–1918.

16 F. Wen, U. Englert, B. Gutrath and U. Simon, *Eur. J. Inorg. Chem.*, 2008, **2008**, 106–111.

17 N. H. Takata, A. M. P. Felicíssimo and V. G. Young Jr, *Inorg. Chim. Acta*, 2001, **325**, 79–84.

18 W. Quintilio, A. Sotelo and A. M. P. Felicissimo, *Spectrosc. Lett.*, 1994, **27**, 605–611.

19 Y. Zhao and D. G. Truhlar, *Theor. Chem. Acc.*, 2008, **120**, 215–241.

20 M. J. Frisch, G. W. Trucks, H. B. Schlegel, G. E. Scuseria, M. A. Robb, J. R. Cheeseman, G. Scalmani, V. Barone, B. Mennucci, G. A. Petersson, H. Nakatsuji, M. Caricato, X. Li, H. P. Hratchian, A. F. Izmaylov, J. Bloino, G. Zheng, J. L. Sonnenberg, M. Hada, M. Ehara, K. Toyota, R. Fukuda, J. Hasegawa, M. Ishida, T. Nakajima, Y. Honda, O. Kitao, H. Nakai, T. Vreven, J. A. Montgomery, J. E. Peralta, F. Ogliaro, M. Bearpark, J. J. Heyd, E. Brothers, K. N. Kudin, V. N. Staroverov, R. Kobayashi, J. Normand, K. Raghavachari, A. Rendell, J. C. Burant, S. S. Iyengar, J. Tomasi, M. Cossi, N. Rega, N. J. Millam, M. Klene, J. E. Knox, J. B. Cross, V. Bakken, C. Adamo, J. Jaramillo, R. Gomperts, R. E. Stratmann, O. Yazyev, A. J. Austin, R. Cammi, C. Pomelli, J. W. Ochterski, R. L. Martin, K. Morokuma, V. G. Zakrzewski, G. A. Voth, P. Salvador, J. J. Dannenberg, S. Dapprich, A. D. Daniels, Ö. Farkas, J. B. Foresman, J. V. Ortiz, J. Cioslowski and D. J. Fox, *Gaussian 09*, Revision C.01, Gaussian, Inc., Wallingford CT, 2009.

21 F. Allen, *Acta Crystallogr., Sect. B: Struct. Sci.*, 2002, **58**, 380–388.

22 T. Dunning Jr and P. Hay, *Mod. Theor. Chem.*, 1977, **3**, 1–28.

23 P. J. Hay and W. R. Wadt, *J. Chem. Phys.*, 1985, **82**, 270–283.

24 P. J. Hay and W. R. Wadt, *J. Chem. Phys.*, 1985, **82**, 299–310.

25 W. R. Wadt and P. J. Hay, *J. Chem. Phys.*, 1985, **82**, 284–298.

26 A. G. Jones and D. B. Powell, *Spectrochim. Acta, Part A*, 1974, **30**, 563–570.

27 G. B. Deacon and J. H. S. Green, *Spectrochim. Acta, Part A*, 1968, **24**, 845–852.